Complex Incompressible Flow Problems

2

Incompressible Flow Solver using Least Square based Artificial Compressibility Method

Mihir Chatterjee*

Chemical Technology Division, Chemical Technology Group, Bhabha Atomic Research Centre (BARC), Trombay – 400085, INDIA

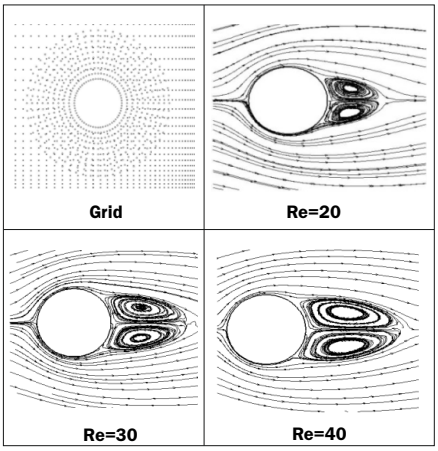

Chimera grid used for computation and streamline plot for flow past a circular cylinder at different Reynolds numbers

ABSTRACT

The objective of the present work is to develop a meshless method based on least square to solve incompressible Navier-Stokes equations. The meshless method based on least square discretization depends on the arbitrary distribution of points called a cloud of points. It requires connectivity and neighbourhood information for every point in the cloud. This study is aimed at applying an upwind differencing scheme in conjunction with the pseudo-compressibility method in meshless framework. Recently meshless methods for several compressible flow algorithms have gained popularity. All meshless numerical methods share a standard feature that no mesh is needed and the solver is capable of operating on an arbitrary distribution of points. For a multibody configuration, clouds of points are generated around every part or component of the body and these clouds around components are then merged to get a distribution of points around it. For completing numerical simulation of Navier-Stokes equations for complex multibody configuration, the generation of an appropriate grid becomes the most difficult job. The pseudo or artificial compressibility method was first introduced by Chorin [1] for solving complex incompressible flow problems. During this formulation, a time derivative of pressure is added to the continuity equation. along with the momentum equations, these form a hyperbolic system of equations, which may be marched in pseudo-time to a steady-state solution. In the present work, an attempt has been made to use the Artificial Compressibility Method (ACM) with meshless least square based discretisation for solving incompressible Navier-Stokes equations. The central idea behind this work is to solve incompressible flow problems using an arbitrary distribution of points or clouds constructed around a geometry applying any available method of grid generation. The advantage of this least square based meshless pseudo-compressibility method is that it is often used to solve incompressible flow problems around complex geometry where the task of grid generation can be simplified by the generation of a cloud of points around the body and their connectivity information.

KEYWORDS: *Navier-Stokes equations, Artificial Compressibility Method*

Introduction

In this paper, least square based meshfree method is used to solve incompressible Navier Stokes equations using the Kinetic theory approach motivated by ACM. ACM was first introduced by Chorin [1] and has been used extensively with much success by Kwak and Kiris [2] for solving complex incompressible flow problems. In this formulation, a time derivative of pressure is added to the continuity equation. Together with the momentum equations, these form a hyperbolic system of equations, which can be marched in pseudo-time to a steady-state solution. The method can also be extended to solve time-dependent problems by using sub-iterations in pseudo time at every physical time step to ensure divergence-free velocity field. If only steady state solution to a problem is required, ACM can be a very efficient formulation because it does not require that divergence–free velocity field be obtained at each iteration but only as the solution converges. Hence ACM is a macroscopic incompressible Navier Stokes (NS) solution method. The addition of the time derivative of pressure to the continuity equation creates a hyperbolic system of equations complete with artificial pressure waves of finite speed. When the solution converges to a steady state, a divergence-free flow field is obtained. Hence many of the well-developed compressible flow algorithms can be utilized for this method.

Ohwada and Asinari [3] have shown the role of kinetic theory in the numerical methods for the Navier-Stokes equation (both compressible and incompressible) with the theory of characteristics for the kinetic equation. They have discussed the relation between ACM and Lattice Boltzmann Method (LBM), which is a kinetic-based method. LBM employs the evolution of microscopic gas models to approximate macroscopic equations of fluid dynamics,as shown by Banda et. al. [4] that yields the solution of Incompressible Navier Stokes Equation (INSE) in the limit Kn~Ma~h→ 0 while only the limit Ma~h→ 0 suffices for ACM. Chatterjee et. al. [5] have used a normal equation approach for incompressible fluid flow using the modified Artificial Compressibility Method (ACM) of Chorin [1] with the least square based discretisation. The present method is based on the principle of Kinetic Theory and ACM using the meshless Kinetic upwind method as adapted by Mahendra et. al. [6].The main aim of this work is *to develop a robust meshfree incompressible flow solver based on kinetic theory.*

**Author for Correspondence: Mihir Chatterjee*
E-mail: mihir@barc.gov.in

Numerical Methods

Golse [7] has given the detailed derivation of Incompressible Navier-Stokes equations from the renormalized solutions of the Boltzmann equation. In the present case incompressibility condition is being simulated by choice of distribution function. Consider the Boltzmann equation with Bhatnagar-Gross-Kook (BGK) model as

$$\frac{\partial f}{\partial t} + \vec{v}\frac{\partial f}{\partial \vec{x}} = J_m(f,f_0) = -\frac{(f - f_0)}{t_R} \quad \text{Eqn.1}$$

where f_0 is the Maxwellian. This equation can also be written in a non-dimensional form as

$$St\left[\frac{\partial f}{\partial t} + \vec{v}\frac{\partial f}{\partial \vec{x}}\right] = -\frac{1}{Kn_L}\frac{(f - f_0)}{\hat{t_R}} \quad \text{Eqn.2}$$

Where $(\hat{t_R}) = t_R v_{th}/\lambda$ and t_R is the dimensionless relaxation time, $v_{th} = 1/\sqrt{\beta}$ is most probable molecular thermal speed. The dimensionless form contains Strouhal number, $St = L_0/t_0 v_{th}$ and local Knudsen number, $Kn_L = \lambda/L_0$ is defined as the ratio of mean free path, λ and length scale, L_0.

The distribution function f for simulation of ACM can be expressed as

$$f = \left(\frac{\rho}{\delta}\right)\left(\frac{\beta}{\pi}\right)^{D/2} exp\,(-\beta\,(\vec{v} - \vec{u})^2) \quad \text{Eqn.3}$$

Where D is the degrees of freedom and pressure p is related to artificial density ρ by the artificial equation of state where δ is the artificial compressibility parameter

$$p = \delta\rho \quad \text{Eqn.4}$$

Now after taking moment we get a set of INSE in Cartesian coordinates.

$$\frac{\partial}{\partial \tau}(U) + \frac{\partial}{\partial x}(GX_I + GX_V) + \frac{\partial}{\partial y}(GY_I + GY_V) = 0 \quad \text{Eqn.5}$$

where,

$$U = \begin{bmatrix} p' \\ u \\ v \end{bmatrix}, GX_I = \begin{bmatrix} \delta u \\ u^2 + p' \\ uv \end{bmatrix}, GY_I = \begin{bmatrix} \delta v \\ uv \\ v^2 + p' \end{bmatrix}, GX_V = \begin{bmatrix} 0 \\ \tau_{xx} \\ \tau_{xy} \end{bmatrix}, GY_V = \begin{bmatrix} 0 \\ \tau_{yx} \\ \tau_{yy} \end{bmatrix} \quad \text{Eqn.6}$$

and p' is the pressure normalized with density. GX_I and GY_I are the x and y component of inviscid flux while GX_V and GY_V are the x and y components of viscous flux respectively. This can be interpreted in a formulation similar to the ACM due to Chorin[1], the continuity equation for incompressible flow is modified by adding a time-derivative of pressure term resulting in:

$$\frac{1}{\delta}\frac{\partial p}{\partial t} + \left(\frac{\partial u}{\partial x} + \frac{\partial v}{\partial y}\right) = 0 \quad \text{Eqn.7}$$

As t no longer represents a true physical time in this formulation, now onwards it is replaced with τ that is an auxiliary variable whose role is analogous to that of time in a compressible flow problem. Hence along with x and y momentum equations (Eqn.9) and (Eqn.10), the modified continuity equation (Eqn.8) forms a hyperbolic system of equations.

$$\frac{1}{\delta}\frac{\partial p}{\partial \tau} + \left(\frac{\partial u}{\partial x} + \frac{\partial v}{\partial y}\right) = 0 \quad \text{Eqn.8}$$

$$\frac{\partial u}{\partial \tau} + \frac{\partial}{\partial x}(p' + uu) + \frac{\partial}{\partial y}(uv) + \frac{\partial}{\partial x}\tau_{xx} + \frac{\partial}{\partial y}\tau_{yx} = 0 \quad \text{Eqn.9}$$

$$\frac{\partial v}{\partial \tau} + \frac{\partial}{\partial x}(uv) + \frac{\partial}{\partial y}(p' + vv) + \frac{\partial}{\partial x}\tau_{xy} + \frac{\partial}{\partial y}\tau_{yy} = 0 \quad \text{Eqn.10}$$

Where,

$$\tau_{xx} = -2\nu\frac{\partial u}{\partial x}, \tau_{yy} = -2\nu\frac{\partial v}{\partial y}, \tau_{xy} = \tau_{yx} = -\nu\left(\frac{\partial u}{\partial y} + \frac{\partial v}{\partial x}\right) \quad \text{Eqn.11}$$

In this formulation the Reynolds stress has been approximated as a function of the strain rate tensor, and thus v represents a sum of the kinematic viscosity and the turbulent eddy viscosity.

Least Square Based Discretization

The present work uses least squares-based discretization due to Ghosh and Deshpande [8], which is a meshless or grid free method. In case of finite difference methods, the above equation is solved by discretizing the various derivatives along the co-ordinate directions. Finite volume method is based on integral form of governing equations. However, if we are given an arbitrary distribution of points without any grid structure associated with these points, it will be difficult to discretize the derivatives. With the least square approach, spatial derivatives f_x, f_y of a function f can be discretized in terms of the data at the neighboring points or nodes. If we consider arbitrary n points (in general it has been observed, for a *2D* or *3D* calculation a minimum of two neighboring nodes per quadrant are required for the least square based discretization) surrounding a point P_o as shown in Fig.1.

The Taylor series around P_o for any quantity f gives us $\Delta f_i = \Delta x_i f_{xo} + \Delta y_i f_{yo}$ + h.o.t.i=1....n, *h.o.t*= higher order terms where $\Delta x_i = x_i - x_o$, $\Delta y_i = y_i - y_o$ and $\Delta f_i = f_i - f_o$. Minimizing the square of error E, defined by

$$E = \sum_{i=1}^{n}(\Delta f_i - \Delta f_{xo}\Delta x_i - \Delta f_{yo}\Delta y_i)^2 \quad \text{Eqn.12}$$

gives the following first order accurate least square formulae for the gradients

$$f_{xo}^{(1)} = \frac{\sum \Delta y_i^2 \sum \Delta x_i \Delta f_i - \sum \Delta x_i \Delta y_i \sum \Delta y_i \Delta f_i}{\sum \Delta x_i^2 \sum \Delta y_i^2 - (\sum \Delta x_i \Delta y_i)^2} \quad \text{Eqn.13}$$

$$f_{yo}^{(1)} = \frac{\sum \Delta x_i^2 \sum \Delta y_i \Delta f_i - \sum \Delta x_i \Delta y_i \sum \Delta x_i \Delta f_i}{\sum \Delta x_i^2 \sum \Delta y_i^2 - (\sum \Delta x_i \Delta y_i)^2} \quad \text{Eqn.14}$$

where Σ represents the summation over all points in the neighborhood $N(P_o)$ of Po. The formulae given in (Eqn. 13) and (Eqn. 14) can now be used to obtain the point values of f_{xo} and f_{yo} throughout the field with incorporation of upwinding.

Incorporation of Upwind Scheme

In the present work upwinding is enforced in least square based discretization method by stencil subdivision. Consider a 2-D linear hyperbolic partial differential equation for scalar f.

$$\frac{\partial f}{\partial t} + v_1\frac{\partial f}{\partial x} + v_2\frac{\partial f}{\partial y} = 0 \quad \text{Eqn.15}$$

The exact solution to this equation is given by

$$f(t + \Delta t, x, y, v_1, v_2) = f(t, x - v_1\Delta t, y - v_2\Delta t, v_1, v_2) \quad \text{Eqn.16}$$

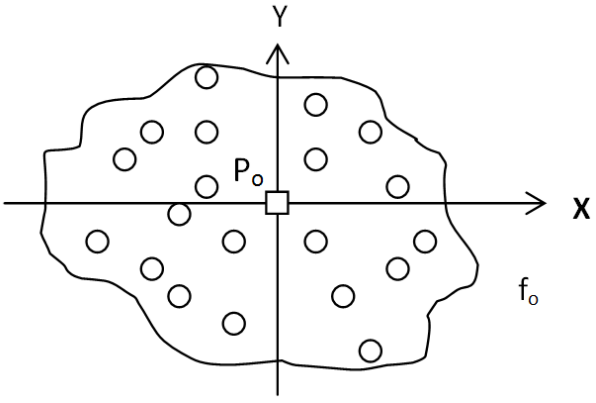

Fig.1: Typical connectivity around point P_o.

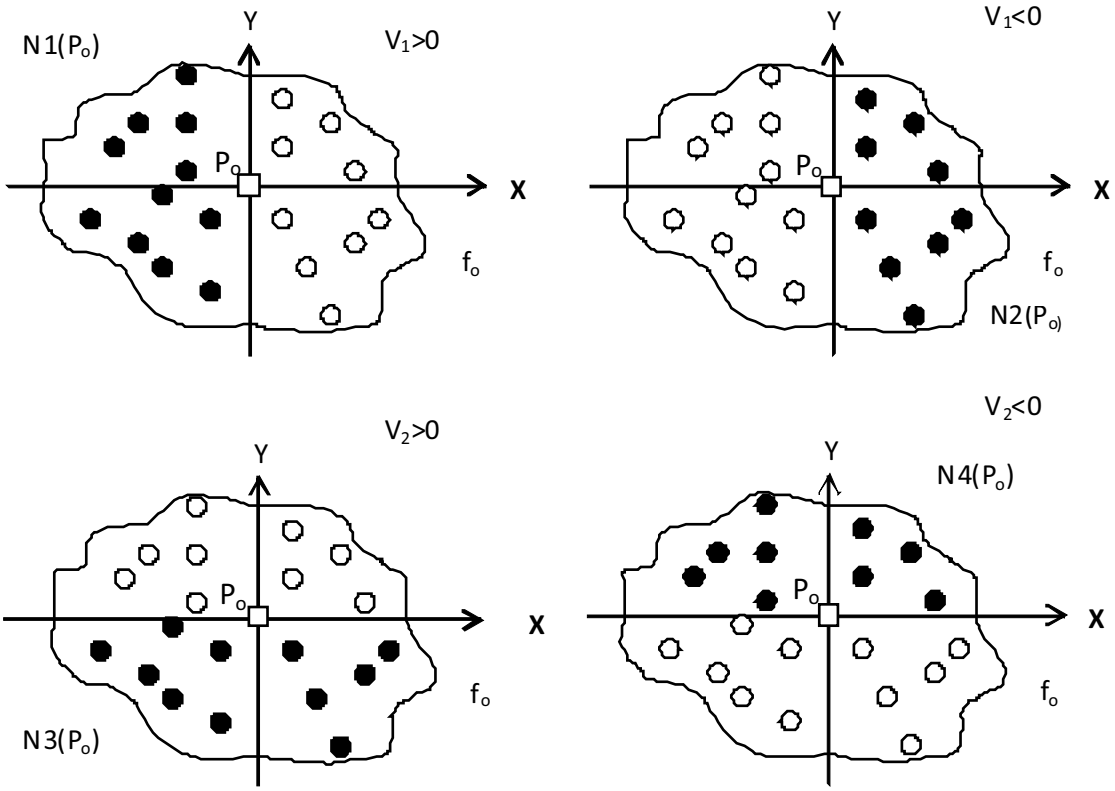

Fig.2: Stencil splitting for Upwinding.

The propagation of information to node Po depends upon location of node P_i relative to P_o and the signs of v_1 and v_2. If v_1> 0 then only the nodes to the left of Po will influence the solution at P_o. Similarly, if v_1< 0 then only the nodes to the right of P_o will influence the solution at P_o. Similar arguments show that for v_2> 0 the node below P_o and for v_2<0 the node above P_o will influence the solution at P_o. For developing any upwind scheme this signal propagation property should be considered. Now replacing the spatial derivative in (Eqn.15) by discrete least square approximation we get

$$\frac{\partial U}{\partial t}+\frac{v_1+|v_1|}{2}\{f_{xo}\}_{N1(P_0)}+\frac{v_1-|v_1|}{2}\{f_{xo}\}_{N2(P_0)}+\frac{v_2+|v_2|}{2}\{f_{yo}\}_{N3(P_0)}+\frac{v_2+|v_2|}{2}\{f_{yo}\}_{N4(P_0)}=0$$

Eqn.17

Where coefficient $\frac{v_1+v_2}{2}$ of the term $\{f_{xo}^{(1)}\}_{N1(p_o)}$ which appears in (Eqn.17) is always positive for v_1>0, while it is zero for v_1<0. This indicates that least square evaluation of derivative

at node Po for v_1>0 should use data at nodes to the left of Po i.e. based on sub stencil N1(P_o)) and is represented as $\{f_{xo}^1\}_{N1(P_o)}$ for v_1>0, $\{f_{xo}^1\}_{N2(P_o)}$ for v_1<0, $\{f_{yo}^1\}_{N3(P_o)}$ for v_2>0, $\{f_{yo}^1\}_{N4(P_o)}$ for v_2<0.

Therefore, based on first order least square update formulation we get the final state update formula for artificial compressibility as follows

$$U^{n+1}=U^n-\Delta\tau\left[\begin{array}{l}\frac{v_1+|v_1|}{2}\left\{\frac{\partial GX}{\partial x}\right\}_{N1(P_0)}+\frac{v_1-|v_1|}{2}\left\{\frac{\partial GX}{\partial x}\right\}_{N2(P_0)}\\+\frac{v_2+|v_2|}{2}\left\{\frac{\partial GY}{\partial y}\right\}_{N3(P_0)}+\frac{v_2+|v_2|}{2}\left\{\frac{\partial GY}{\partial y}\right\}_{N4(P_0)}\end{array}\right]$$

Eqn.18

Where,

$$\left\{\frac{\partial}{\partial x}(GX)\right\}_{N1(P_o)}^n=\left[\frac{\sum_i\Delta y_i^2\sum_i\Delta x_i\Delta(GX)_i^n-\sum_i\Delta x_i\Delta y_i\sum_i\Delta y_i\Delta(GX)_i^n}{\sum_i\Delta x_i^2\sum_i\Delta y_i^2-\left(\sum_i\Delta x_i\Delta y_i\right)^2}\right]_{\in N1(P_o)}$$

Eqn.19

$$\left\{\frac{\partial}{\partial x}(GX)\right\}_{N2(P_o)}^n=\left[\frac{\sum_i\Delta y_i^2\sum_i\Delta x_i\Delta(GX)_i^n-\sum_i\Delta x_i\Delta y_i\sum_i\Delta y_i\Delta(GX)_i^n}{\sum_i\Delta x_i^2\sum_i\Delta y_i^2-\left(\sum_i\Delta x_i\Delta y_i\right)^2}\right]_{\in N2(P_o)}$$

Eqn.20

$$\left\{\frac{\partial}{\partial x}(GY)\right\}_{N3(P_o)}^n=\left[\frac{\sum_i\Delta x_i^2\sum_i\Delta y_i\Delta(GY)_i^n-\sum_i\Delta x_i\Delta y_i\sum_i\Delta x_i\Delta(GY)_i^n}{\sum_i\Delta x_i^2\sum_i\Delta y_i^2-\left(\sum_i\Delta x_i\Delta y_i\right)^2}\right]_{\in N3(P_o)}$$

Eqn.21

$$\left\{\frac{\partial}{\partial x}(GY)\right\}_{N4(P_o)}^n=\left[\frac{\sum_i\Delta x_i^2\sum_i\Delta y_i\Delta(GY)_i^n-\sum_i\Delta x_i\Delta y_i\sum_i\Delta x_i\Delta(GY)_i^n}{\sum_i\Delta x_i^2\sum_i\Delta y_i^2-\left(\sum_i\Delta x_i\Delta y_i\right)^2}\right]_{\in N4(P_o)}$$

Eqn.22

where $\Delta(GX)_i^n=(GX)_i^n-(GX)_o^n$ and $\Delta(GY)_i^n=(GY)_i^n-(GY)_o^n$, and GX (=$GX_l$+$GX_v$) and GY(=$GY_l$+$GY_v$) represent the split fluxes for incompressible flow.

Code Validation

The benchmark problem of flow past a circular cylinder and backward facing step have been chosen in the present study to validate the code. In principle, the concept of mesh-free least square-based discretization works well for "any mesh" system, in which the nodes can be either regularly or irregularly distributed. This provides the present mesh free method geometric flexibility.

Flow Past Circular Cylinder

The nodes in the neighborhood of the circular cylinder are generated under the cylindrical coordinate system as shown in Fig.3a. This cylindrical mesh is fused with an underlying Cartesian mesh and a Chimera grid is appropriately generated. In the present study, we have performed numerical simulation at a series of Reynolds number from 20 to 40 with various flow patterns in the steady state. In all cases, a pair of vortices develop behind the cylinder and is perfectly aligned as

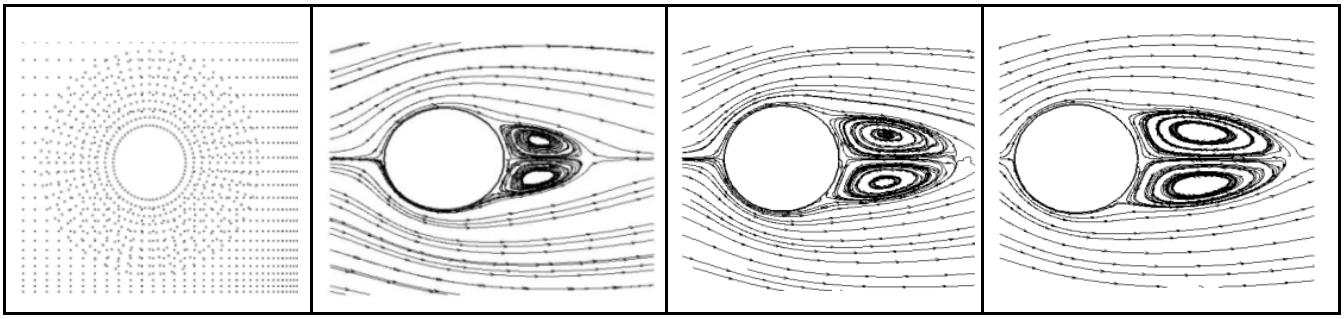

Fig.3: Chimera grid used for computation and streamline plot for flow past a circular cylinder at different Reynolds numbers.

shown in Fig.3 for different Reynolds number. This is consistent with the experimental observation.

Some quantitative parameters for the re-circulating region, such as the length of the re-circulating region L_{sep}, from the rearmost point of the cylinder to the end of the wake, separation angle θ_{sep} are shown in the Fig.4. The results from the present calculation as well as the result of the other researchers are listed in table 1 for the test case of Reynolds number of 20 and 40. Here C_d is the drag coefficient. All these flow parameters agree well with the results of previous studies for the Reynolds number studied.

Backward Facing Step Problem

Fluid flows in channels with flow separation and reattachment of the boundary layers are encountered in many flow problems like heat exchangers and ducts. Among this type of flow problems, a backward facing step can be regarded as having a simple geometry while retaining rich flow physics manifested by flow separation, flow reattachment and multiple recirculating zones in the channel depending on the Reynolds number. The geometrical parameters are step height, channel height and channel length. This problem has been used as a validation test case. The challenge in modelling this problem comes from the fact that the sizes of the separation zones downstream of the step are very sensitive to the pressure gradient in the flow, especially when the boundary layer is separated. If separation is present, a pressure wave traveling with finite speed will cause a change in the local pressure gradient, which will affect the location of the flow separation. It has been observed that this change in separated flow will cause a feed back to the pressure field, possibly preventing convergence to a steady state. The geometry used in the calculation is shown in Fig.5, where 's' is the height of the step. The entrance channel width is equal to the step height and its length is double the step height. The total length of the channel from the step is 30s.

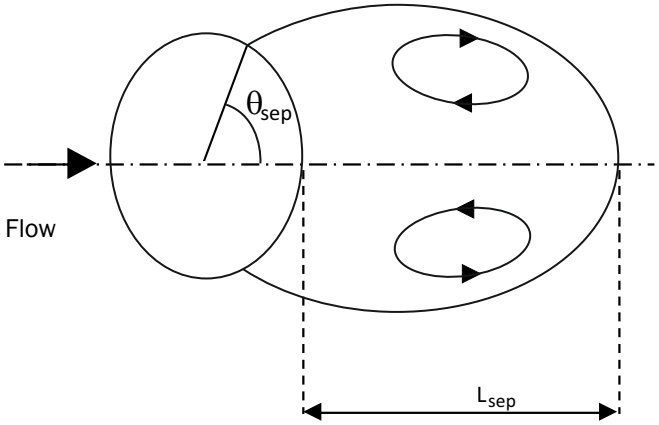

Fig.4: Characteristic parameters of the cylinder wake.

In a very important study Yee et al. [13] observed the spurious behavior of the numerical schemes. They showed that for backward facing step flow when a coarse grid mesh is used, one can obtain a spurious oscillating numerical solution. Erturk [14] have reported that when a finer mesh was used, the oscillating behavior of the numerical solution disappeared and it was possible to obtain a steady solution. They stated that when finer grids are used, the Mesh Reynolds number defined as $Re_m = u\Delta h/v$ decreases and this improves the numerical stability characteristics of the numerical scheme used, and allows high Reynolds number flows computable. In the present study, a fine unstructured mesh is used in order to obtain steady state numerical solutions. A part of the unstructured grid used for computation is shown in Fig.6.

At the inflow boundary, it is assumed that the flow is fully developed plane Poiseuille flow between parallel plates such that a parabolic velocity profile is prescribed throughout the calculation, and the static pressure is allowed to change. No

Table 1: Comparison of parameters for flow past circular cylinder.

	Re=20			Re=40		
Source	L_{sep}	q_{sep}	C_d	L_{sep}	q_{sep}	C_d
Dennis and Chang *[9]*	0.94	43.7	2.05	2.35	53.8	1.522
Takami and Keller *[10]*	0.935	43.7	2.05	2.32	53.6	1.536
Tuann and Olson *[11]*	0.9	44.1	2.25	2.1	54.8	1.675
Ding et. al. *[12]*	0.93	44.1	2.18	2.20	53.5	1.713
Present	0.94	43.7	2.08	2.11	54.4	1.795

Fig.5: Outline of the backward facing step problem.

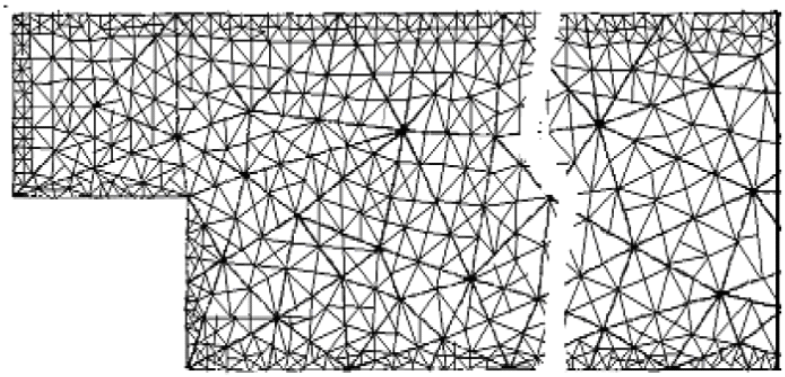

Fig.6: Outline of the backward facing step problem.

slip boundary condition is prescribed at the top and bottom wall. Two step heights downstream from the inflow a two to one expansion is encountered. The outflow boundary extends to 30 step heights downstream of the step. At this exit boundary a outflow boundary condition has been used. The flow was calculated using a grid of total 24600 points. The grid is unstructured and clustered near the side boundary for better resolution of the flow features to be captured.

The streamline plots for different Reynolds numbers are shown in Fig.7. It is observed from the plots that as the Reynolds number increases the length of the primary separation zone x_1 also increases. At Reynolds number = 400 a secondary separation zone has been developed at the top wall boundary.

A set of experimental and numerical solutions found in the literature has been compared with the present computational result in order to demonstrate the accuracy of the present numerical solutions. Armaly et al. [15] have experimentally obtained the u-velocity profile at several x-locations (plotted as a fraction of the total length of the configuration S, i.e x/S) for Reynolds number Re=100 for a backward facing step. For the same geometry a numerical solution for a steady two-dimensional flow is also presented by Erturk [14]. The u-velocity profiles at the corresponding x-locations drawn to the same scale for this experimental and computed results are shown in the figure 8 and are compared with u-velocity profiles at the same x locations from the simulation with the present method. From Fig.8 it can be seen that the present computed velocity profiles agree well (except at the immediate downstream of the step) with that of experimental results of Armaly et al. [15] and numerical result of Erturk [14]. The difference at the flow separation zone is attributed to the feedback effect of pressure wave.

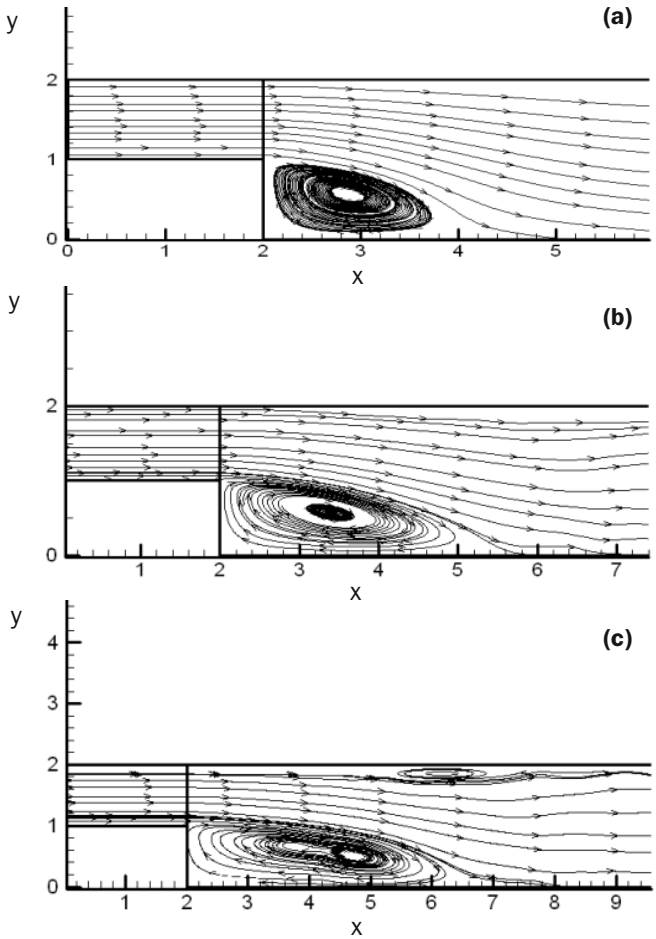

Fig.7: Streamline plot for flow over a backward facing step at Reynolds number a.100 b.200 and c.400.

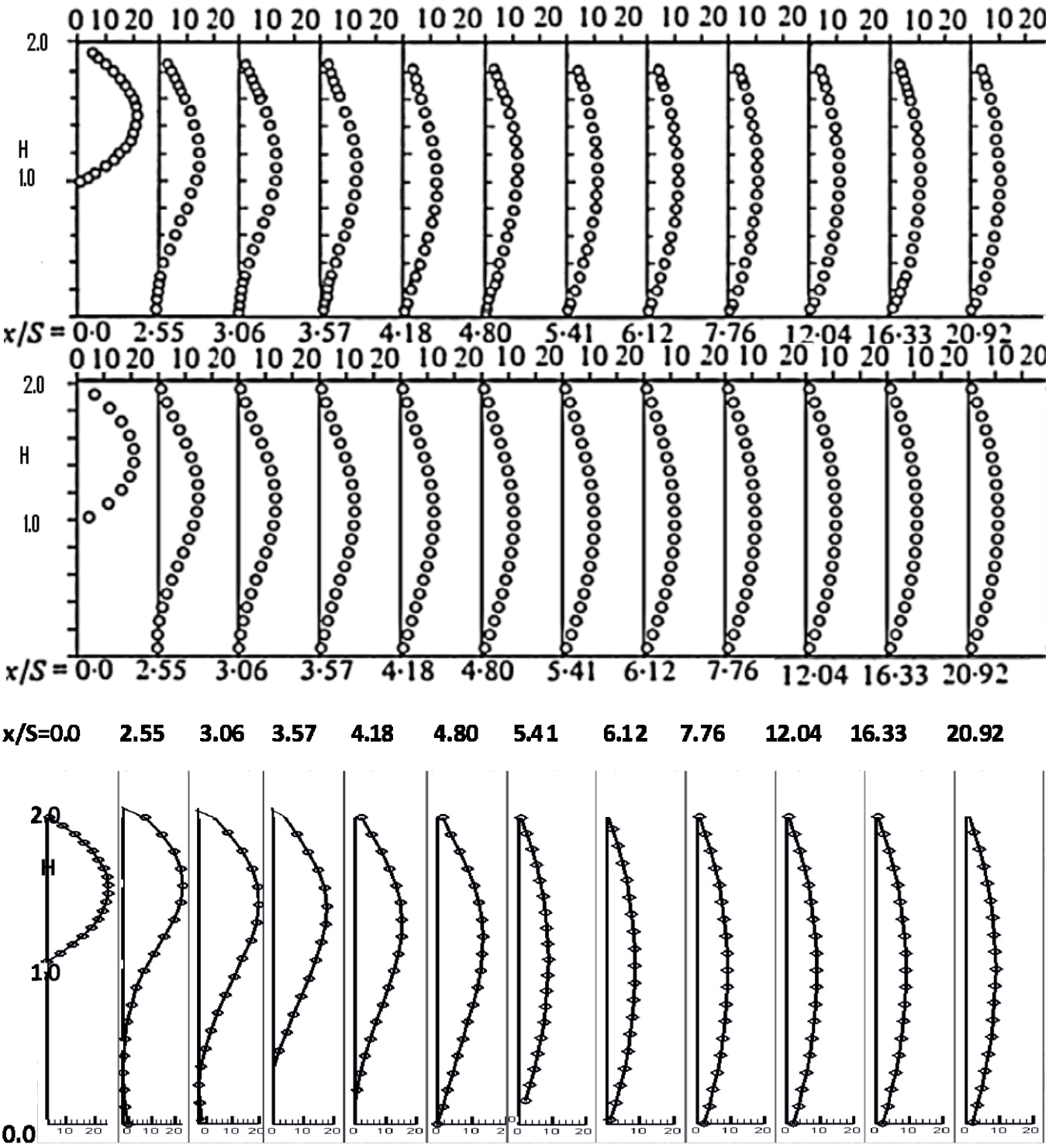

Fig.8: u-velocity profiles at various downstream locations for Re=100; Top figure Armaly et.al [15], middle figure Erturk [14], bottom figure present study.

Conclusions

A Kinetic Upwinding theory-based approach motivated by the Artificial Compressibility Method for the solution of the incompressible Navier-Stokes equations using meshfree least square based discretization has been developed. Numerical simulations were carried out for two incompressible benchmark flow problems. The obtained numerical results agree well with the results published in literature.

Acknowledgements

The author acknowledges the requisite technical support provided by M. S. Deshpande, Head, Chemical Technology Division (ChTD), BARC; Vinay Kumar, Scientific Officer (G), ChTD and Chandrajit Singh Chauhan, Scientific Officer (D), ChTD.

References

[1] Chorin A. J. "Numerical Solution of the Navier-Stokes Equations", Mathematics and Computers, 22(1968), 742- 762.

[2] Kwak D., Kiris C. "Computational Challenges of Viscous incompressible Flows", Computers and Fluids, 34(2005) 283-299.

[3] Ohwada T, Asinari P., "Artificial Compressibility Method Revisited, Asymptotic Numerical Method for Incompressible Navier-Stokes Equations", Journal of Computational Physics, 229(5)(2010)1698-1723.

[4] Banda M. K., Junk M., Klar A. "Kinetic-based Numerical Schemes for Incompressible Navier–Stokes Equations", Computers and Fluids, 35(2006)879–887.

[5] Chatterjee M., Mahendra A. K., Sanyal A., Gouthaman G, "A Mesh Free Method for Simulations of Incompressible Fluid Flow", Computer Modeling in Engineering & Sciences, 83 (4)(2012)385-402.

[6] Mahendra A. K., Singh R. K., Gouthaman G, "Meshless Kinetic Upwind Method for Compressible, Viscous Rotating Flows", Computers and Fluids, 46(1)(2010)325-332.

[7] Golse F. "From the Boltzmann Equation to the Incompressible Navier-Stokes Equations", Proceedings of Symposia of Applied Mathematics, 65(2007)355-366.

[8] Ghosh A. K., Deshpande S. M., "Least Squares Kinetic Upwind Method for Inviscid Compressible Flows", AIAA Paper 95 (1995), 1001-1011.

[9] Dennis S. C. R., Chang G. Z., "Numerical Solutions for Steady Flow Past a Circular Cylinder at Reynolds Number up to 100", Journal of Fluid Mechanics, 42(1970)471-489.

[10] Takami H., Keller H. B., "Steady Two-dimensional Viscous Flow of an Incompressible Fluid Past a Circular Cylinder", Physics of Fluids 12 (Suppl II) (1969)II-51-63.

[11] Tuann S. Y.; Olson M. D., "Numerical Studies of the Flow around a Circular Cylinder by a Finite Element Method", Computers and Fluids, 6(1978) 219-240.

[12] Ding H., Shu C., Yeo K. S., Xu D., "Simulation of Incompressible Viscous Flows Past a Circular Cylinder by Hybrid FD Scheme and Meshless Least Square-based Finite Difference Method" Computer Methods in Applied Mechanical Engineering, 193(2004)727-744.

[13] Yee H. C., Torezymski J. R., Mortan S. A., Visbal M. R., "On Spurious Behavior of CFD Simulations", International Journal for Numerical Methods in Fluids, 30 (1999)675-711.

[14] Erturk E., "Numerical Solutions of 2-D Steady Incompressible Flow over a Backward-Facing Step, Part I: High Reynolds Number Solutions", Computers and Fluids, 37 (2008) 633-655.

[15] Armaly B. F., Durst F., Periera J. C. F., Schonung B., "Experimental and Theoretical Investigation of Backward-facing Step Flow", Journal of Fluid Mechanics, 127(1983)473-496.

Notations

Symbol	Description	Unit
β	$M/2RT$	s^2/m^2
δ	Artificial compressibility parameter	Pa. m^3/Kg
Δf_i	$f_i - f_o$	-
Δx_i	$x_i - x_o$	m
Δy_i	$y_i - y_o$	m
θ_{sep}	Separation angle	Degree
λ	Mean free path	m
τ_{ij}	Components of shear stress on the i^{th} plane in j^{th} direction	Pa
ρ	Artificial density	Kg/m^3
τ	Pseudo time	-
ν	Sum of the kinematic viscosity and the turbulent eddy viscosity	m^2/s
C_d	Dimensionless Drag coefficient	-
D	Degrees of freedom	-
E	Error	-
f	Distribution function for ACM	-
f_0	Maxwellian probability distribution function	-
$f_{xo}^{(1)}$	First order accurate least square formula for x derivative of function f at point P_o	-
$f_{yo}^{(1)}$	First order accurate least square formula for y derivative of function f at point P_o	-
GX_I	x component of inviscid flux	-
GX_V	x component of viscous flux	-
GY_I	y component of inviscid flux	-
GY_I	y component of viscous flux	-
h	Mesh spacing	m
Kn	Dimensionless Knudsen Number	-
L_0	Length scale	m
L_{sep}	Length of the re-circulating region	m
Ma	Dimensionless Mach Number	-
p	Pressure	Pa
R	Universal gas Constant	J/(K.mole)
Re	Dimensionless Reynolds Number	-
s	Step height	m
S	Total length of backward facing step configuration	m
St	Dimensionless Strouhal number	-
t	Time	s
T	Temperature in absolute scale	K
t_R	Dimensionless relaxation time	-
u	x component of velocity	m/s
U	State vector	-
v	y component of velocity	m/s
v_{th}	Most probable molecular thermal speed	m/s